UNITED STATES DEPARTMENT OF THE INTERIOR

GEOLOGICAL SURVEY

A Direct Method for Calculating Instrument Noise Levels in Side-by-Side Seismometer Evaluations

by

L. Gary Holcomb

Open-File Report 89-214

This report is preliminary and has not been reviewed for conformity with U.S. Geological Survey editorial standards. Any use of trade names is for descriptive purposes only and does not imply endorsement by the U.S. Geological Survey.

Albuquerque, New Mexico

1989

Table of Contents

1 INTRODUCTION ..... 1 - 1

2 HISTORY ..... 2 - 1

3 MODEL MATHEMATICAL RELATIONSHIPS ..... 3 - 1
3.1 BASIC MODEL EQUATIONS ..... 3 - 1
3.2 SOLUTION OF MODEL EQUATIONS ..... 3 - 2

4 COHERENCE ..... 4 - 1

5 MODEL PERFORMANCE ON DUMMY NOISE DATA ..... 5 - 1

6 MODEL PERFORMANCE ON REAL TEST DATA ..... 6 - 1

7 CONCLUSIONS AND RECOMMENDATIONS ..... 7 - 1

8 REFERENCES ..... 8 - 1

A APPENDIX ..... A - 1

Table of Figures

Block diagram of test configuration ..... 3 - 1
Minimum SNR's at low coherence levels ..... 4 - 2
Minimum SNR's at high coherence levels ..... 4 - 2
Raw N1 PSD estimates ..... 5 - 1
Raw N2 PSD estimates ..... 5 - 1
Confidence Limits as a function of Degrees of Freedom ..... 5 - 2
N1 PSD estimates with supersmoothing (SNR = 1) ..... 5 - 3
N2 PSD estimates with supersmoothing (SNR = 1) ..... 5 - 3
N1 PSD estimates with supersmoothing (SNR = 1) ..... 5 - 4
N2 PSD estimates with supersmoothing (SNR = 32) ..... 5 - 4
N1 PSD estimates with supersmoothing (PSD = 32) ..... 5 - 5
N2 PSD estimates with supersmoothing (SNR = 32) ..... 5 - 5
PSD estimates for V349 and V350 ..... 6 - 1
Raw N1 PSD estimates for V349 ..... 6 - 2
Raw N2 PSD estimates for V350 ..... 6 - 2
Coherence between V349 and V350 ..... 6 - 3
N1 PSD estimates without smoothing with equalization ..... 6 - 4
N2 PSD estimates without smoothing with equalization ..... 6 - 4
Smoothing function used to supersmooth noise estimates ..... 6 - 5
N1 PSD estimates with equalization and with supersmoothing ..... 6 - 6
N2 PSD estimates with equalization and with supersmoothing ..... 6 - 6
Coherent power estimates between V349 and V350 ..... 6 - 7
PSD estimates for Guralp systems ..... 6 - 8
PSD estimates for Streckeisen systems ..... 6 - 8
Coherence between Guralp sensors ..... 6 - 9
Coherence between Streckeisen sensors ..... 6 - 9
Noise estimate for H377 ..... 6 - 10
Noise estimates for H376 ..... 6 - 10
Noise estimates for S1E ..... 6 - 10
Noise estimates for S2E ..... 6 - 10
Coherent power estimate between H377 and H376 ..... 6 - 11
Coherent power estimate for S1E and S2E ..... 6 - 11
Estimate of dynamic range of noise estimates ..... 6 - 11
Diagram of test configuration including recording noise ..... A - 1
Diagram of test configuration with recording noise at input ..... A - 3

1 INTRODUCTION

The subject of determining the inherent system noise levels present in modern broadband closed loop seismic sensors has been an evolving topic ever since closed loop systems became available. Closed loop systems are unique in that the system noise can not be determined via a blocked mass test as in older conventional open loop seismic sensors. Instead, most investigators have resorted to performing measurements on two or more systems operating in close proximity to one another and to analyzing the outputs of these systems with respect to one another to ascertain their relative noise levels.

The analysis of side-by-side relative performance is inherently dependent on the accuracy of the mathematical modeling of the test configuration. This report presents a direct approach to extracting the system noise levels of two linear systems with a common coherent input signal. The mathematical solution to the problem is incredibly simple; however the practical application of the method encounters some difficulties. Examples of expected accuracies are presented as derived by simulating real systems performance using computer generated random noise. In addition, examples of the performance of the method when applied to real experimental test data are shown.

2 HISTORY

Here at the Albuquerque Seismological Laboratory (ASL), closed loop systems have been evaluated for over 17 years. Normally, instruments of the same manufacturer with closely matched frequency response functions whose internal noise levels were approximately equal were the subjects of these investigations at ASL. A system model describing these conditions was derived (see Peterson *et al.* 1980) and applied to numerous closed loop system evaluations over those 17 years. In addition, this model was occasionally applied to instruments whose characteristics were significantly different.

Other agencies have also evaluated closed loop systems; they have used various linear system models to process their data. The net result is that test results may not be directly comparable between agencies because the analysis depends on the assumptions which were made in modeling the systems.

Recently, the need to conduct evaluations between instruments from different manufacturers has become a more frequent requirement. The assumptions of closely matched frequency response functions and approximately equal noise levels, which was made in the model derived above, does not necessarily hold if one is testing instruments from different manufacturers.

In addition, ASL recently became involved in a mutual test and evaluation program with other agencies in which the direct comparison of test results is necessary. It was obviously time to take a fresh look at the models used to evaluate closed loop systems and to attempt to obtain a general model applicable to all systems. In the process of analyzing the general case, it was discovered that, since the objective of most evaluations was the noise levels of the systems under test, the solution to the problem is relatively simple and straight forward.

3 MODEL MATHEMATICAL RELATIONSHIPS

The system to be evaluated is modeled in Figure 3.1 where X is assumed to be the coherent ground motion power spectral density (PSD) input to both systems. All quantities in the figure are assumed to be functions of frequency. Experimentally, the observer does not know X, N_1, and N_2; the signals appearing at ports 1 and 2 are the only two time functions whose PSD functions (P_{11} and P_{22}) are available for measurement and analysis. In addition, the system transfer functions (H_1 and H_2) are assumed to be known. The circle containing "S" denotes a summing junction.

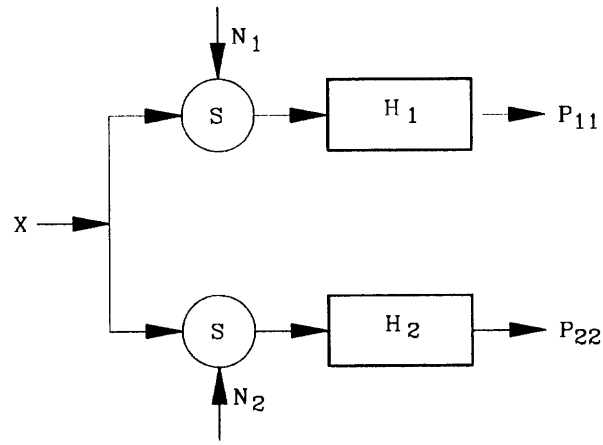

Figure 3.1 Linear system model of side-by-side evaluation of two seismometer systems.

3.1 BASIC MODEL EQUATIONS

Figure 3.1 contains a block diagram depicting the configuration of two seismometer systems operating in close enough proximity to one another that the seismic signal input power X may be assumed to be at the same level and coherent between the sensors. The two systems are assumed to have system transfer functions H_1 and H_2 which are not necessarily equal. In addition the sensors are assumed to be generating incoherent self noise powers N_1 and N_2 referred to the input, not necessarily equal.

The relationships between power at various points in the block diagram in Figure 3.1 can be written in terms of system equations which relate the power outputs from the systems to the power appearing at the inputs of the systems. The power spectral density of the output of system 1 is given by

$$P_{11} = |H_1|^2 [X + N_1] \qquad \textit{Equation} \quad 3.1$$

and the same quantity for system 2 is

$$P_{22} = |H_2|^2 [X + N_2] \qquad \textit{Equation} \quad 3.2$$

The cross spectral density between the outputs of the two systems may be written as

$$P_{12} = H_1 H_2^* X \qquad \textit{Equation} \quad 3.3$$

3.2 SOLUTION OF MODEL EQUATIONS

The solution of these three equations depends on the desired information one needs to acquire. In the case of test and evaluation of two seismometers operating side-by-side, one frequently needs estimates of the noise levels associated with the subject instruments. This information can easily be obtained directly from the three equations without resorting to intermediate definitions of additional quantities such as the coherence function or the signal-to-noise ratio (SNR) as follows. Simply solve Equation 3.1 for N_1 to yield

$$N_1 = \frac{P_{11}}{|H_1|^2} - X \qquad \textit{Equation} \quad 3.4$$

Substituting for X from Equation 3.3 yields

$$N_1 = \frac{P_{11}}{|H_1|^2} - \frac{P_{12}}{H_1 H_2^*} \qquad \textit{Equation} \quad 3.5$$

Similarly, solving Equation 3.2 for N_2 and substituting for X from Equation 3.3 yields

$$N_2 = \frac{P_{22}}{|H_2|^2} - \frac{P_{12}}{H_1 H_2^*} \qquad \textit{Equation} \quad 3.6$$

The two system noise power spectra in Equations 3.5 and 3.6 are expressed in terms of directly measurable quantities at the outputs of the two test systems and the system transfer functions. These two equations are simply the expression that the incoherent noise power (P_{noise}) is equal to the total system output power (P_{total}) minus the coherent input power ($P_{coherent}$).

$$P_{noise} = P_{total} - P_{coherent} \qquad \textit{Equation} 3.7$$

or the more familiar expression

$$P_{total} = P_{coherent} + P_{noise} \qquad \textit{Equation} 3.8$$

4 COHERENCE

Since the system noise spectra can be derived directly, as has been demonstrated above, the question arises as to the utility of the coherence function. The coherence function can be used to make preliminary estimates of the systems SNR's and to place lower limits on the SNR's as will now be shown.

The coherence function is defined as (see Bendat and Piersol, 1971 p 32)

$$\gamma^2 = \frac{|P_{12}|^2}{P_{11}P_{22}} \qquad \textit{Equation} \quad 4.1$$

Substituting for P_{11}, P_{22}, and P_{12} from equations 3.1, 3.2, and 3.3 respectively yields

$$\gamma^2 = \frac{|H_1 H_2^* X|^2}{|H_1|^2 [X + N_1]\, |H_2|^2 [X + N_2]} \qquad \textit{Equation} \quad 4.2$$

The response functions divide out of the expression leaving

$$\gamma^2 = \frac{X^2}{X^2 + X(N_1 + N_2) + N_1 N_2} \qquad \textit{Equation} \quad 4.3$$

Inverting, multiplying both sides by X^2, and dividing both sides by N_1N_2 yields

$$\frac{1}{\gamma^2}\frac{X^2}{N_1N_2} = \frac{X^2}{N_1N_2} + \frac{X}{N_2} + \frac{X}{N_1} + 1 \qquad \textit{Equation} \quad 4.4$$

Rearranging we have

$$\frac{X}{N_1}\frac{X}{N_2}\left(1 - \frac{1}{\gamma^2}\right) + \frac{X}{N_1} + \frac{X}{N_2} + 1 = 0 \qquad \textit{Equation} \quad 4.5$$

This expression relates the power SNR's of the two channels to the coherence and it is in the form of the general equation of an equilateral hyperbola. Figure 4.1 presents the interrelationship of the two channel SNR's for 9 values of coherence spaced 0.1 apart and Figure 4.1 extends the plot to high values of coherence extending from 0.90 to 0.99.

The asymptotes to these hyperbolas are given by

$$\frac{X}{N_1} = \frac{X}{N_2} = \frac{\gamma^2}{1 - \gamma^2} \qquad \textit{Equation} \quad 4.6$$

Therefore, given a value of the coherence between the output signals of a side-by-side test of two instruments, the power SNR's in both instruments must be at least as high as the value given by Equation 4.6. Since it is unlikely that, under low background conditions, the SNR on one instrument will greatly exceed that in the other if the PSD's are somewhat equal, the plots in Figures 4.1 and 4.2 can be used to obtain quick estimates of the system SNR's.

The special case of equal SNR's in both channels can be analyzed by letting $N_1 = N_2$ ($\frac{X}{N_2} = \frac{X}{N_2}$) in Equation 4.5 and solving for the quadratic for the SNR. The root is found to be

$$\frac{X}{N_1} = \frac{X}{N_2} = \frac{\gamma}{1-\gamma} \qquad \textit{Equation} \quad 4.7$$

This condition is the special case of equal noise in both sensors which was modeled at ASL earlier (see Peterson *et al.* 1980).

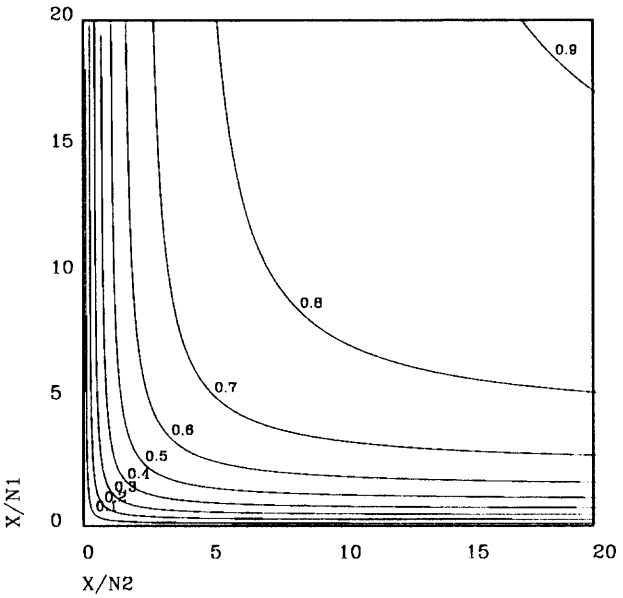

Figure 4.1 The interrelationship of the channel power SNR's and coherence at low levels of coherence.

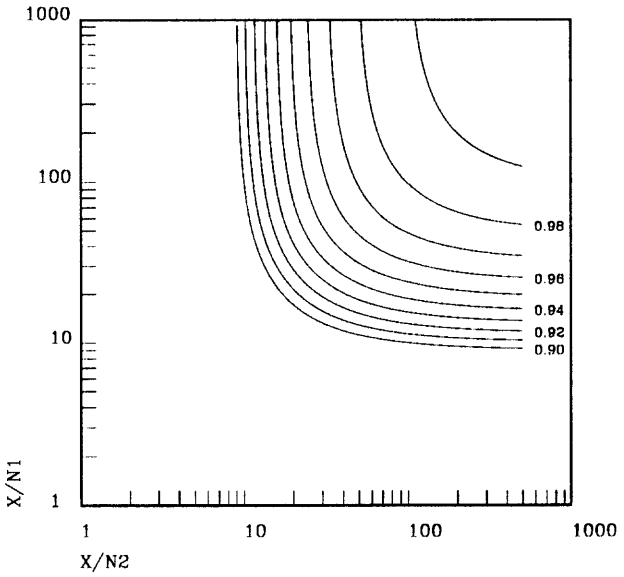

Figure 4.2 The interrelationship of the channel power SNR's and coherence at high levels of coherence.

For convenience, representative minimum SNR's (the asymptotes to the hyperbolas) pertaining to a series of coherence values are tabulated in Table 4.1.

Coh	Min SNR	Coh	Min SNR	Coh	Min SNR
0.1	0.1	0.91	10.1	0.991	110.1
0.2	0.3	0.92	11.5	0.992	124.0
0.3	0.4	0.93	13.3	0.993	141.9
0.4	0.7	0.94	15.7	0.994	165.7
0.5	1.0	0.95	19.0	0.995	199.0
0.6	1.5	0.96	24.0	0.996	249.0
0.7	2.3	0.97	32.3	0.997	332.3
0.8	4.0	0.98	49.0	0.998	499.0
0.9	9.0	0.99	99.0	0.999	998.9

Table 4.1 Tabulation of minimum possible SNR values for various coherence levels. These numbers are the asymptotes to the hyperbolas in Figures 4.1 and 4.2 corresponding to the values of coherence listed.

5 MODEL PERFORMANCE ON DUMMY NOISE DATA

The performance of this simple model has been evaluated by applying it to the analysis of artificially generated data whose power levels are accurately known. A random number generator (see Stearns 1988, pp.52-54) was used to create uncorrelated time sequences to represent N_1, N_2, and X whose power spectral density levels were accurately known. Both N_1 and N_2 were the summed with X to create time sequences with known amounts of coherent and incoherent power. For the first test configuration H_1 and H_2 were considered to both be equal to 1.

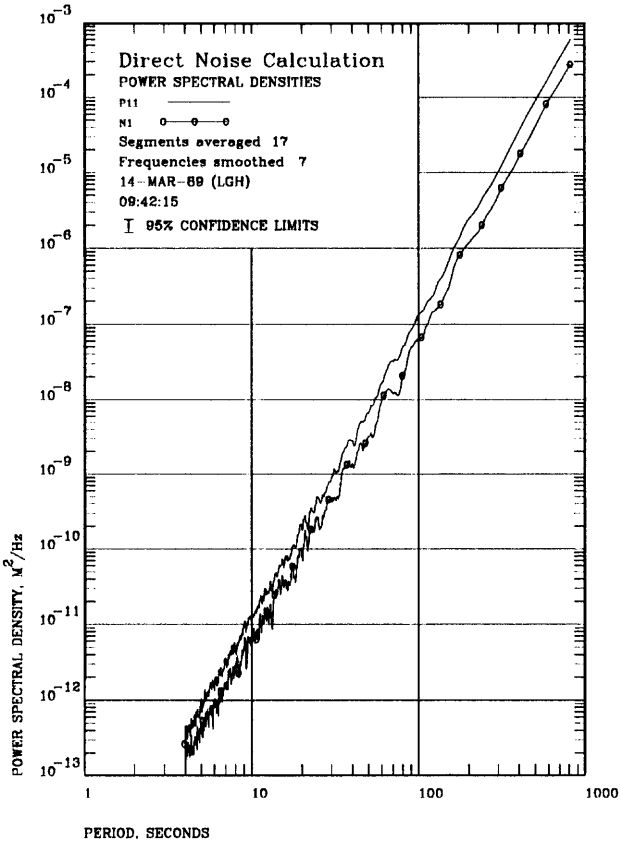

Figure 5.1 PSD estimates for the total power (P11 = 2) and the noise power (N1 = 1) in the first channel (SNR = 1).

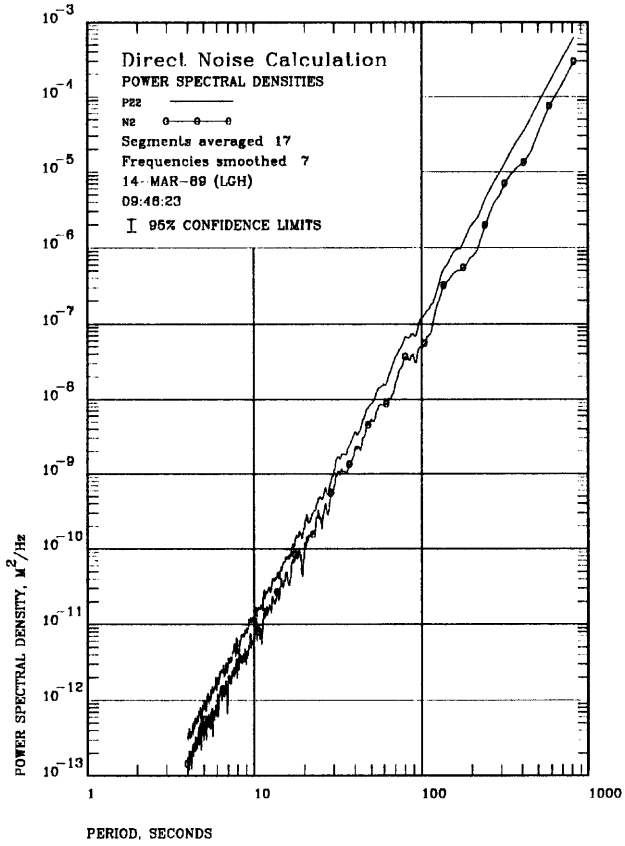

Figure 5.2 PSD estimates for the total power (P22 = 2) and the noise power (N2 = 1) in the second channel (SNR = 1).

Figures 5.1 and 5.2 contain the results of the analysis process when the input powers were all equal ($X = N_1 = N_2 = 1$). These parameters yield a SNR of 1 for both channels. The plotted

PSD estimates have been treated as though they were instrument acceleration output spectra corrected to real displacement ground motion; therefore they are not flat as one would expect for white noise. Instead, the slope of the plots closely resembles the noise output of noisy seismic sensors as will be apparent below.

Note that most of the PSD estimate plots herein contain a 95% confidence limit bar at the bottom of the title block. This error bar is provided to give the reader an approximate idea of the probable error in the estimates. It is plotted with a fixed length associated with data with 224 degrees of freedom in all figures. All spectral estimates used to perform the calculations in Equations 3.4, 3.5, and 3.6 had at least 224 degrees of freedom obtained by smoothing over 7 frequencies in the frequency domain (see Bendat & Piersol 1971, pp.327-329) followed by averaging over 16 segments. Further smoothing will increase the number of degrees of freedom but, as Figure 5.5 (replotted here from the table in Munk *et al.* 1959, p.291) indicates, the change in the confidence limits as the number of degrees of freedom increases beyond 224 is not great. Therefore, a fixed length 224 degrees of freedom error bar has been plotted in all figures.

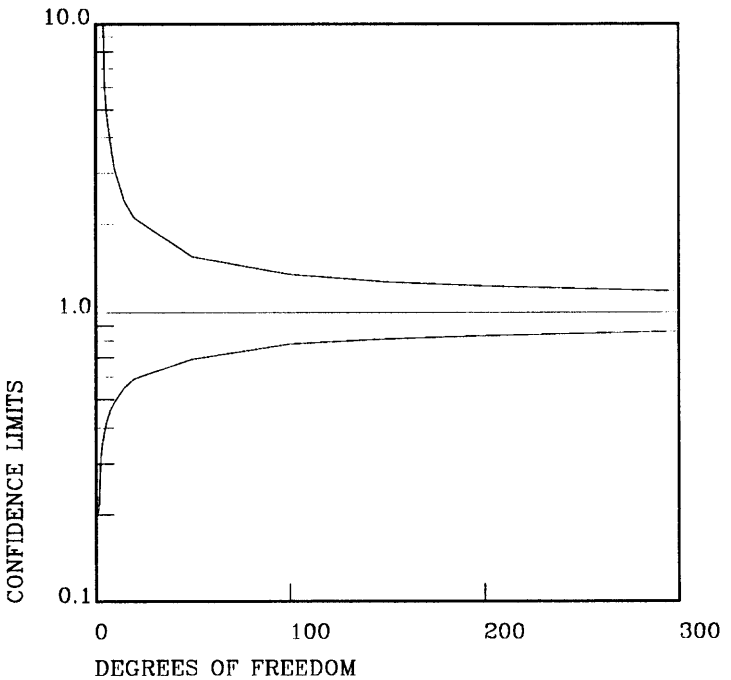

Figure 5.3 The dependence of the 95% confidence limits on the number of degrees of freedom.

The individual spectra in Figures 5.1 and 5.2 are rather rough particularly at short periods. Additional smoothing would make the plots more appealing to the eye; in addition, experiments at higher SNR's revealed that more smoothing increased the accuracy of the estimates of the noise levels. Therefore, Figures 5.4 and 5.5 present the same data as Figures 5.1 and 5.2 after a significantly greater degree of smoothing. The added smoothing will be referred to as "super-smoothing" in this paper. Note that much of the jitter at short periods has been evened out and the relationship between the two PSD estimates is much clearer in the second two figures.

The justification for and the type of smoothing operation chosen comes in the realm of what the author will refer to as "spectral gardening". No attempt will be made to rigorously justify it mathematically. Instead, the author will cut and trim the PSD estimates as needed to make the process work! The details of and partial justification for the smoothing operation used to create Figures 5.4 and 5.5 will be presented in Section 6.

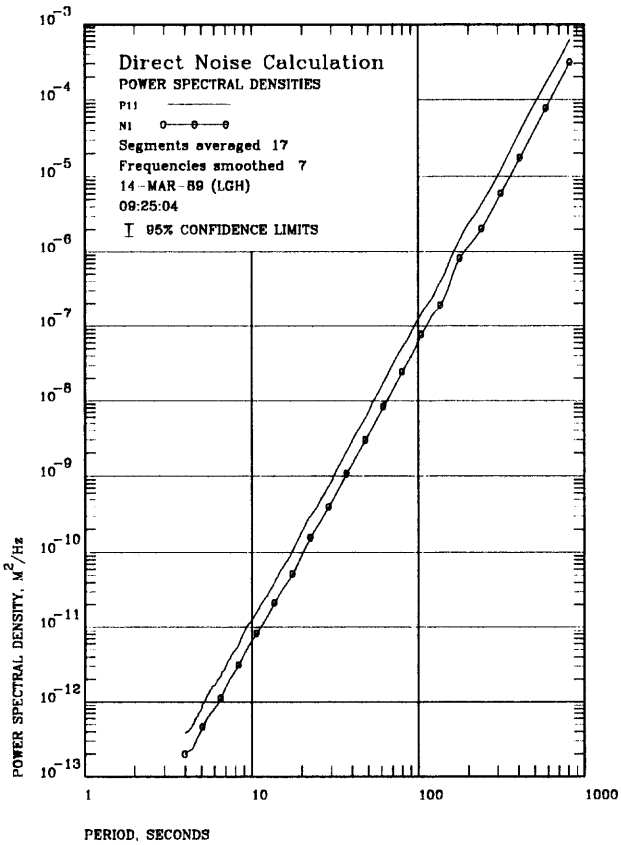

Figure 5.4 PSD estimates for the total power (P11 = 2) and the noise power (N1 = 1) in the first channel with supersmoothing.

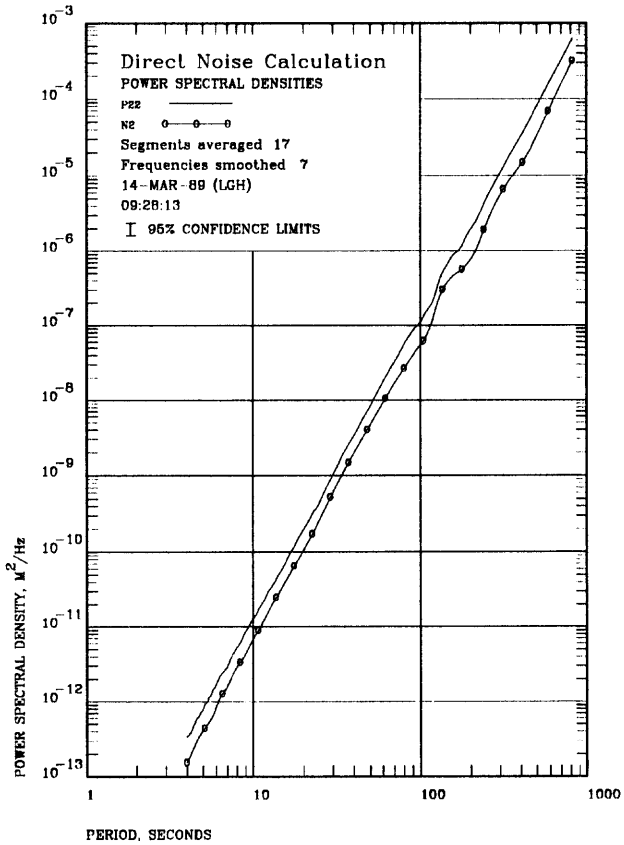

Figure 5.5 PSD estimates for the total power (P22 = 2) and the noise power (N2 = 1) in the second channel with supersmoothing.

The supersmoothed estimates in Figures 5.4 and 5.5 agree very closely with what one should expect. The estimated total power in both channels (P_{11} and P_{22}) is approximately twice as high as the estimates for the noise in each channel as it should be. When averaged over the entire band (4 to 4096 seconds), the estimate of the noise power in the first channel (N_1) is 5.8 % lower than it theoretically should be, and the estimate of the noise power in the second channel (N_2) is 1.4 % too low (see the first line of table 5.1). The averaged estimated SNR for channel 1 was calculated to be 0.927 and for channel 2 it was 0.905 (theoretically they should both be 1). Obviously, the estimated SNR is not equal to these numbers across the entire band because the

PSD estimates are not perfectly white; variations do exist particularly at longer periods. However, the variations lie well within the probable confidence limits shown in the header of the figures.

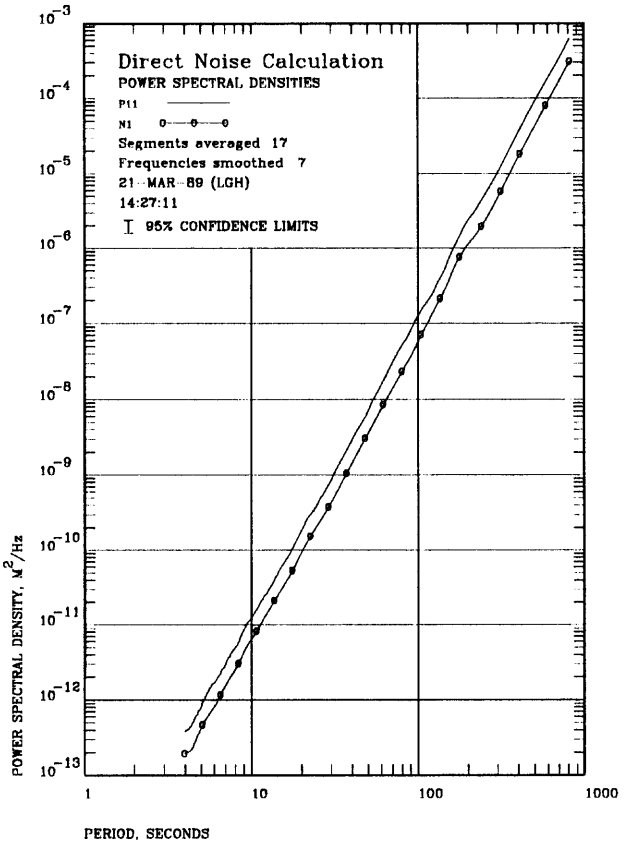

Figure 5.6 PSD estimates for the total power (P11 = 2.0) and the noise power (N1 = 1.0) in the first channel (SNR = 1) with supersmoothing.

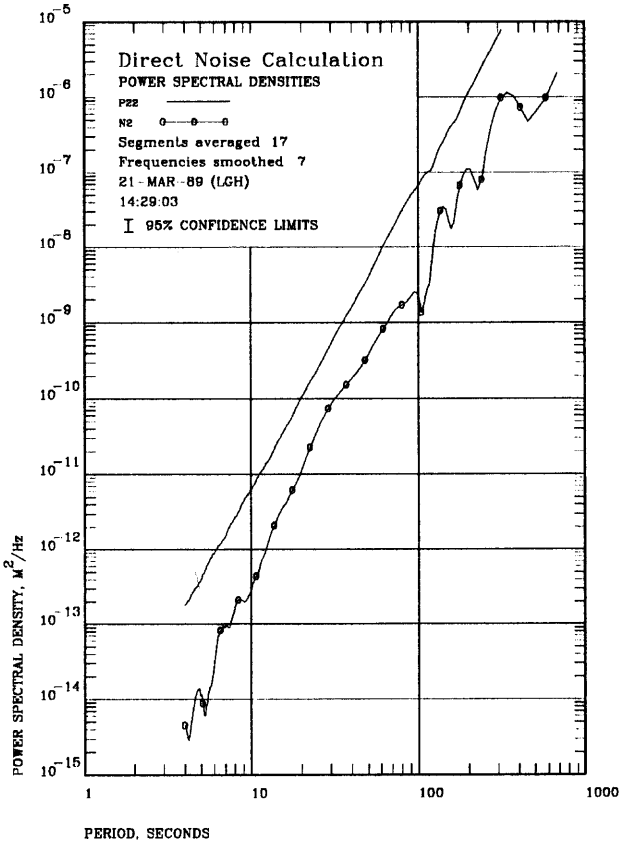

Figure 5.7 PSD estimates for the total power (P11 = 1.03125) and the noise power (N1 = 0.03125) in the second channel (SNR = 32) with supersmoothing.

Figures 5.6 and 5.7 contain the results of direct model processing of data from two channels with significantly different SNR's. The results are not as accurate as were those for the equal SNR case but they are readily usable. The averaged estimate of the first channel noise level is 6.9 % lower than theoretically predicted while the averaged estimate of the second channel noise level is 67.3 % higher than predicted (see line one of Table 5.6). The averaged estimated SNR for channel 1 was 1.007 and for channel 2 it was 15.95 (theoretically, the first SNR should have been 1 and the second should have been 32). The error in the estimates for channel 2 are larger than one should expect; possibly other samples of noise would yield better results. Despite the decline in accuracy, the analysis process shows that channel 1 is definitely noisier than channel 2 and it gives a credible estimate of the noise levels in each channel.

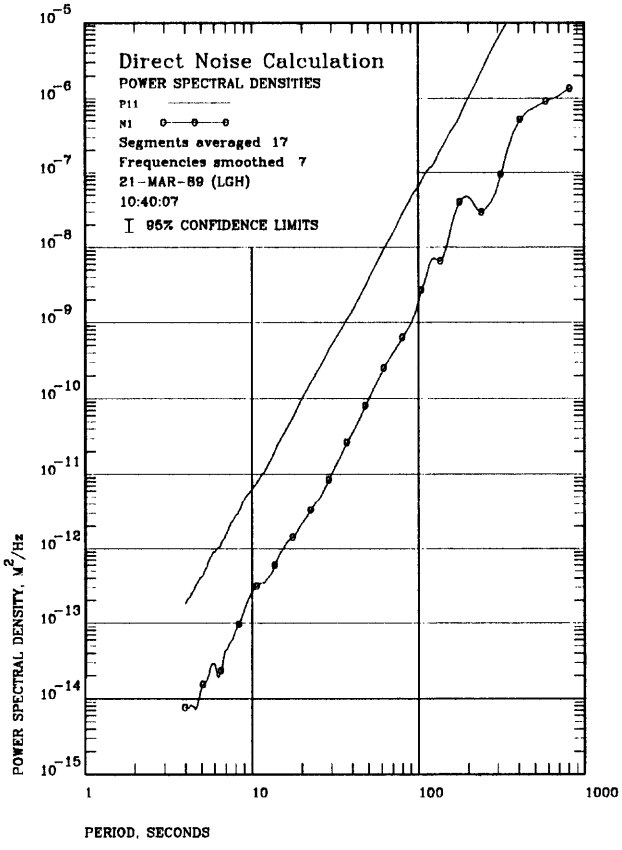

Figure 5.8 PSD estimates for the total power (P11 = 1.03125) and the noise power (N1 = 0.03125) in the first channel (SNR = 32) with supersmoothing.

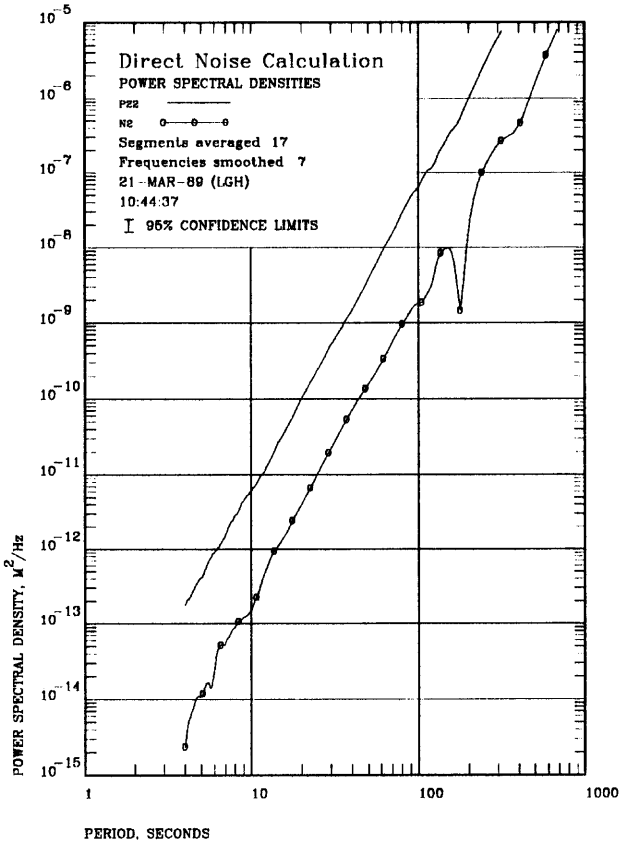

Figure 5.9 PSD estimates for the total power (P22 = 1.03125) and the noise power (N2 = 0.03125) in the second channel (SNR = 32) with supersmoothing.

Figures 5.8 and 5.9 contain the results of direct model analysis of two low noise channels. The PSD estimates for the averaged noise level in channel 1 are 5.2 % lower than theoretically predicted while the estimates for the averaged noise level in channel 2 are 18.3 % lower than predicted (see the last line of Table 5.6). The averaged estimated SNR for channel 1 is 29.9 and for channel 2 it was 32.9 (theoretically they both should have been equal to 32). These estimates are quite remarkable considering the branch of mathematical science used to derive them (the statistical analysis of random processes).

Tables 5.1 through 5.6 contain complete summaries of the model performance in analyzing dummy data at various combinations of SNR levels extending from a SNR of 1 to a SNR of 32. The real power levels listed in the tables were calculated from the original random time series (see Stearns 1988, pp.52-54). The calculated estimates of the PSD levels were made by averaging each PSD over the entire range of the estimate (1024 data points extending from 4 to 4096 seconds). The % err is the % deviation between the calculated PSD of the original random time

series and the average of the PSD estimates obtained by applying the direct model analysis. Therefore, the % error figures are average deviations over the entire band; the error at any given period may be greater or less than the number shown.

The data in the first line of each table corresponds to a channel 1 SNR of 1, the second line corresponds to a channel 1 SNR of 2, the third line corresponds to a channel 1 SNR of 4, the fourth line corresponds to a channel 1 SNR of 8, the fifth line corresponds to a channel 1 SNR of 16, and the sixth line corresponds to a channel 1 SNR of 32.

X real	X calc	X % err	N1 real	N1 calc	N1 % err	N2 real	N2 calc	N2 % err
0.989	0.962	-2.8	1.038	0.977	-5.8	1.063	1.048	-1.4
0.989	0.986	-0.3	0.522	0.486	-6.9	1.063	1.038	-2.4
0.989	0.993	0.4	0.263	0.239	-9.2	1.063	1.021	-4.0
0.989	0.982	-0.7	0.133	0.127	-4.6	1.063	1.009	-5.2
0.989	0.972	-1.8	0.068	0.079	16.6	1.063	1.000	-5.9
0.989	0.972	-1.7	0.035	0.050	42.2	1.063	1.000	-6.0

Table 5.1 Summary of direct model performance in analyzing dummy data ($X = 1, N_1 =$ variable, $N_2 = 1, SNR_2 = 1$).

X real	X calc	X % err	N1 real	N1 calc	N1 % err	N2 real	N2 calc	N2 % err
0.989	0.966	-2.4	1.038	0.973	-6.2	0.537	0.537	0.1
0.989	0.986	-0.3	0.522	0.486	-6.9	0.537	0.526	-2.0
0.989	0.992	0.3	0.263	0.240	-9.0	0.537	0.514	-4.2
0.989	0.984	-0.5	0.133	0.125	-6.0	0.537	0.505	-5.9
0.989	0.977	-1.2	0.068	0.074	8.2	0.537	0.497	-7.3
0.989	0.978	-1.2	0.035	0.043	24.6	0.537	0.497	-7.4

Table 5.2 Summary of direct model performance in analyzing dummy data ($X = 1, N_1 =$ variable, $N_2 = 0.5, SNR_2 = 2$).

X real	X calc	X % err	N1 real	N1 calc	N1 % err	N2 real	N2 calc	N2 % err
0.989	0.968	-2.1	1.038	0.970	-6.5	0.272	0.281	3.3
0.989	0.986	-0.3	0.522	0.486	-6.8	0.272	0.269	-1.1
0.989	0.991	0.2	0.263	0.240	-8.8	0.272	0.261	-4.0
0.989	0.985	-0.4	0.133	0.124	-7.0	0.272	0.254	-6.6
0.989	0.981	-0.8	0.068	0.070	2.4	0.272	0.247	-9.1
0.989	0.981	-0.8	0.035	0.039	12.6	0.272	0.246	-9.4

Table 5.3 Summary of direct model performance in analyzing dummy data ($X = 1, N_1 =$ variable, $N_2 = 0.25, SNR_2 = 4$).

X real	X calc	X % err	N1 real	N1 calc	N1 % err	N2 real	N2 calc	N2 % err
0.989	0.970	-1.9	1.038	0.968	-6.7	0.138	0.152	10.1
0.989	0.986	-0.3	0.522	0.486	-6.8	0.138	0.140	1.2
0.989	0.991	0.2	0.263	0.241	-8.7	0.138	0.134	-3.2
0.989	0.986	-0.3	0.133	0.123	-7.7	0.138	0.128	-7.2
0.989	0.983	-0.6	0.068	0.067	-1.6	0.138	0.123	-11.4
0.989	0.984	-0.5	0.035	0.036	4.4	0.138	0.122	-11.8

Table 5.4 Summary of direct model performance in analyzing dummy data ($X = 1, N_1 =$ variable, $N_2 = 0.125, SNR_2 = 8$).

X real	X calc	X % err	N1 real	N1 calc	N1 % err	N2 real	N2 calc	N2 % err
0.989	0.972	-1.7	1.038	0.967	-6.8	0.071	0.089	24.9
0.989	0.986	-0.3	0.522	0.487	-6.8	0.071	0.075	6.1
0.989	0.991	0.2	0.263	0.241	-8.6	0.071	0.070	-0.6
0.989	0.987	-0.2	0.133	0.123	-8.2	0.071	0.066	-7.2
0.989	0.985	-0.4	0.068	0.065	-4.4	0.071	0.061	-14.0
0.989	0.986	-0.3	0.035	0.034	-1.3	0.071	0.060	-14.9

Table 5.5 Summary of direct model performance in analyzing dummy data ($X = 1, N_1 =$ variable, $N_2 = 0.0625, SNR_2 = 16$).

X real	X calc	X % err	N1 real	N1 calc	N1 % err	N2 real	N2 calc	N2 % err
0.989	0.973	-1.6	1.038	0.966	-6.9	0.037	0.061	67.3
0.989	0.986	-0.3	0.522	0.487	-6.8	0.037	0.046	24.7
0.989	0.991	0.2	0.263	0.241	-8.5	0.037	0.040	8.6
0.989	0.987	-0.2	0.133	0.122	-8.5	0.037	0.035	-5.4
0.989	0.987	-0.2	0.068	0.064	-6.4	0.037	0.031	-16.5
0.989	0.987	-0.2	0.035	0.033	-5.2	0.037	0.030	-18.3

Table 5.6 Summary of direct model performance in analyzing dummy data ($X = 1, N_1 =$ variable, $N_2 = 0.03125, SNR_2 = 32$).

6 MODEL PERFORMANCE ON REAL TEST DATA

Analyzing data obtained from a real world test situation is more difficult than was the artificial data case. Obviously, because the answer is unknown, it is harder to determine if the analysis process is producing meaningful estimates of system parameters. The spectra are not white; instead they extend over several decades in power thereby limiting the degree with which they may be smoothed.

Data obtained during the test and evaluation of a set of three component Guralp CMG-3 borehole sensors will be used to illustrate the practical analysis of real data. This data was chosen because source files were still available on the ASL computer system disks thereby facilitating easy processing. The PSD estimates obtained for the two vertical sensors (serial numbers V349 and V350) is shown in Figure 6.1. Note that one sensor (V349) was considerably noisier than the other, and that both sensor PSD estimates lie above the quiet site noise model shown as a heavy line near the bottom of the figure. Both sensors had only recently been installed and had not been allowed to settle down. Therefore, the data presented herein should not be considered as indicative of the true performance capabilities of the instruments involved; instead, it should be regarded as a readily available source of time series on which to demonstrate the direct model analysis process under discussion herein.

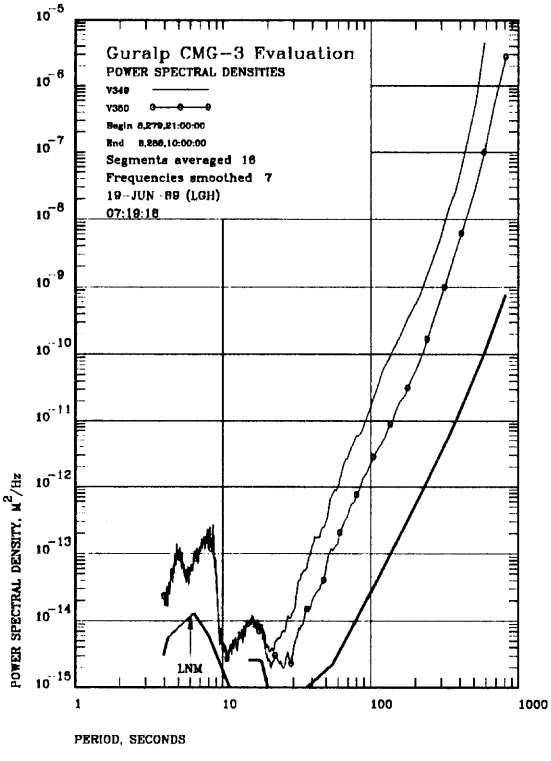

Figure 6.1 PSD estimates (P11 and P22) for vertical sensor modules V349 and V350.

The results of the direct application of Equations 3.4 and 3.5 to analyze the noise levels in modules V349 and V350 are shown in Figures 6.2 and 6.3. The indicated levels of noise lie well below the total powers in both channels below approximately 20 seconds. The ratio of the total power to the noise power is about 20 below 10 seconds.

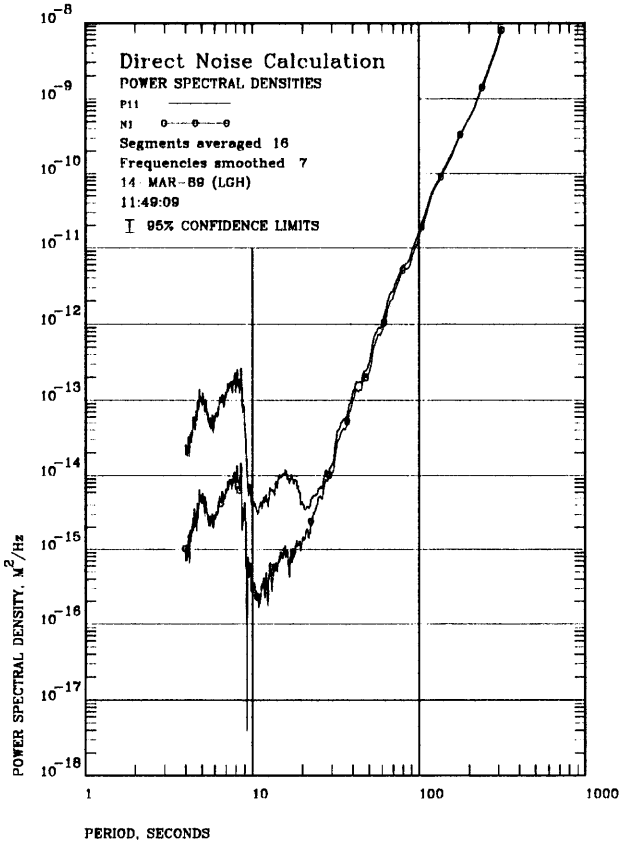

Figure 6.2 PSD estimates for N1 without equalization and without supersmoothing.

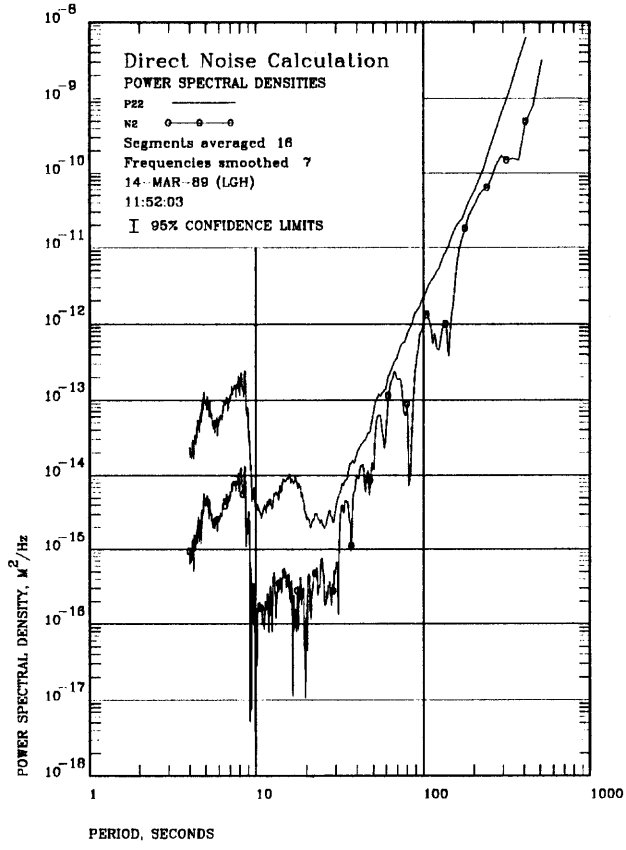

Figure 6.3 PSD estimates for N2 without equalization and without supersmoothing.

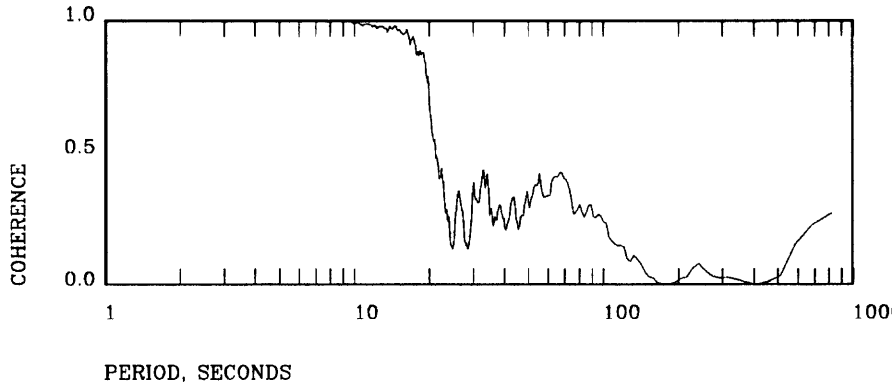

Figure 6.4 Coherence between CMG-3 modules V349 and V350.

However, the coherence between these two sensors shown in Figure 6.4 would suggest that this ratio should be greater because the coherence lies well above 0.9 over this frequency range. High coherence (γ^2 greater than 0.9) indicates that most of the total power is coherent power (ground motion); therefore, the ratio of the total power to the noise power is approximately equal to the SNR and this should be considerably greater than 20 (see Section 4). Tabulated values for the coherence (not contained herein) between 4 and 9 seconds revealed a minimum of 0.9832, a maximum of 0.9998, and an average of 0.997 for the coherence over that period range. Comparing these numbers with Table 4.1 predicts that the SNR should be somewhere around 332, not 20.

Therefore, the results of directly applying equations 3.4 and 3.5 to the analysis of real test data appear to be in error. The most probable source of error is in the precision with which the two system transfer functions are known. Even very small errors in the transfer function will translate into relatively large errors in the calculated noise level because, at high coherence values, Equations 3.4 and 3.5 involve taking the differences between what should be nearly equal PSD estimates. A small error in the transfer function creates PSD estimates which are abnormally distinct and in turn translates into a false indication of high noise in the sensor.

Therefore, the gains of the two sensors were equalized by determining the average ratio of the PSD's over the range in which the coherence is high (4 to 9 seconds) and then adjusting one of the spectra to a level to make this ratio equal to 1. The resulting noise estimates are shown in Figures 6.4 and 6.5.

Notice that the calculated SNR for both sensors is now approximately 100 or greater in the 4 to 9 second range after channel gain equalization as apposed to 20 before equalization. This level of SNR agrees much better with the high coherence values shown in Figure 6.4. The ratio in the transfer functions used to adjust the PSD's in this case was only 1.05; therefore an apparent 5% error in the system gains translated into a very large error in the estimated noise levels.

The PSD estimates for N_1 and N_2 in Figures 6.5 and 6.6 are very noisy and indefinite themselves. It is evident that further smoothing would make things much neater. Several smoothing algorithms were tried with varying success. A very attractive low-pass filter via the Fast Fourier Transform algorithm (see Press *et al.* pp.495-497) worked beautifully on the dummy white noise

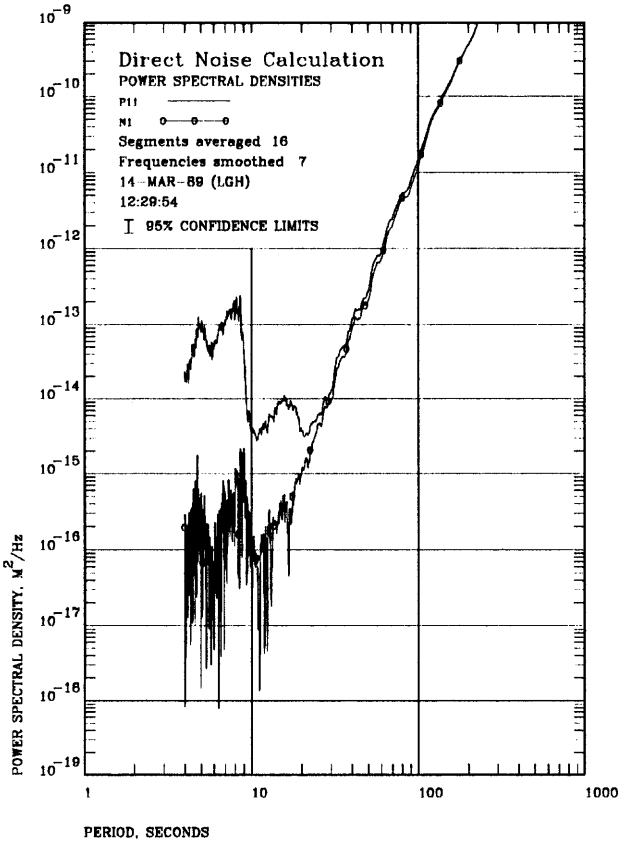

Figure 6.5 PSD estimates for N1 with equalization but without supersmoothing.

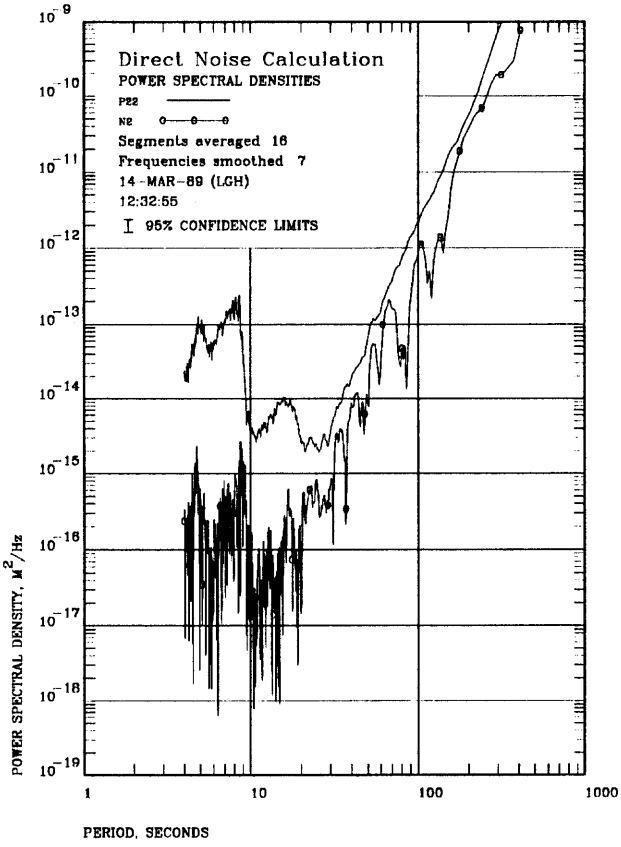

Figure 6.6 PSD estimates for N2 with equalization but without supersmoothing.

analysis of Section 5 but failed miserably when applied to the real data of this section. It appeared that the windowing process in the algorithm was unable to resolve the extended dynamic range in the real data; possibly a different window such as the Taylor window would cure the problem. This approach is mentioned here because the author feels that it shows promise if further refined.

The algorithm finally chosen to supersmooth the PSD was a refinement of smoothing in the frequency domain (see Bendat & Piersol pp.327-329) in which a least squares fit to the data points lying below and above a particular PSD data point are used to calculate a smoothed value for that data point instead of merely averaging the data points. The crux of this type of process is the choice of how many adjacent data points to include in calculating the smoothed value for each data point. The data in Figures 6.5 and 6.6 indicate that more smoothing is necessary at shorter periods because the noise data (N_1 and N_2) are much more ragged at shorter periods and because the density of data points is greater in that portion of the figures. After several empirical tests, the following parameters were found to produce reasonable results on real data.

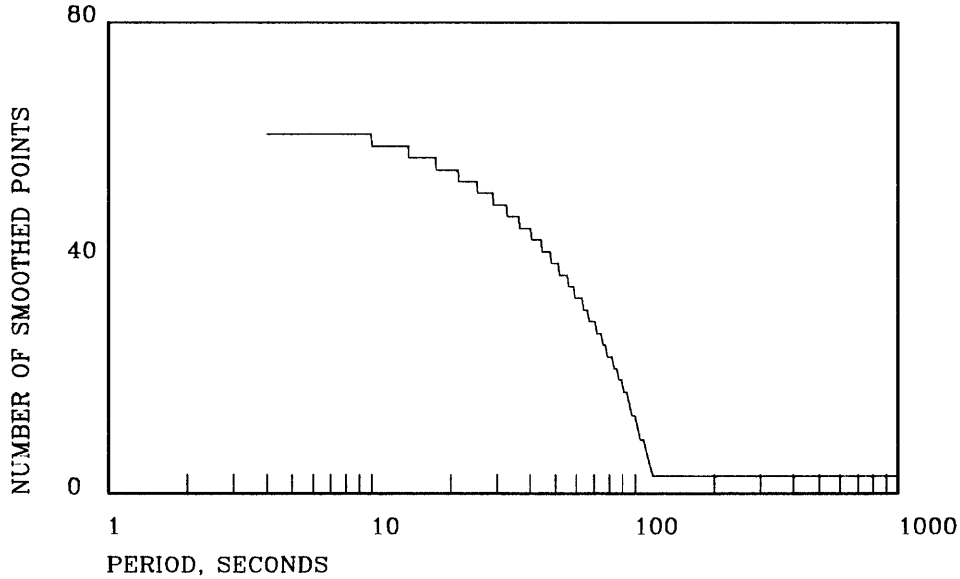

Figure 6.7 Number of points included in supersmoothing as function of period.

Each data point below 10 seconds was smoothed with the 30 data points both lying immediately above and below it. The number of data points included in the smoothing operation for data points lying between 10 and 120 seconds was variable starting with 30 at 10 seconds and decreasing linearly with period to 1 at 120 seconds. Above 120 seconds, the number included was constant at 1 above and 1 below the point being smoothed. The total number of data points included in each smoothing operation is depicted in Figure 6.7. The details of this smoothing algorithm are not critical; the parameters can probably be varied considerably without significant changes in the results.

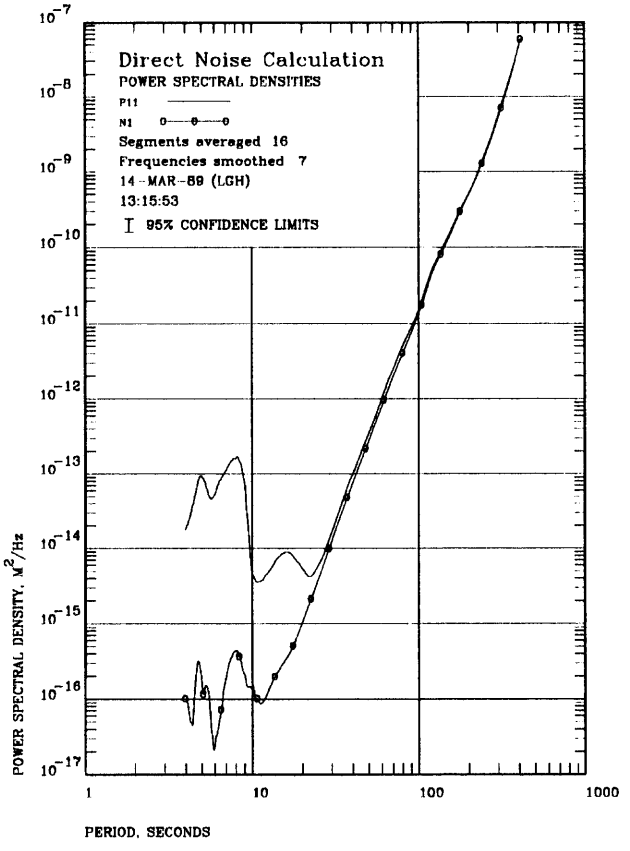

Figure 6.8 N1 PSD estimates with equalization and with supersmoothing.

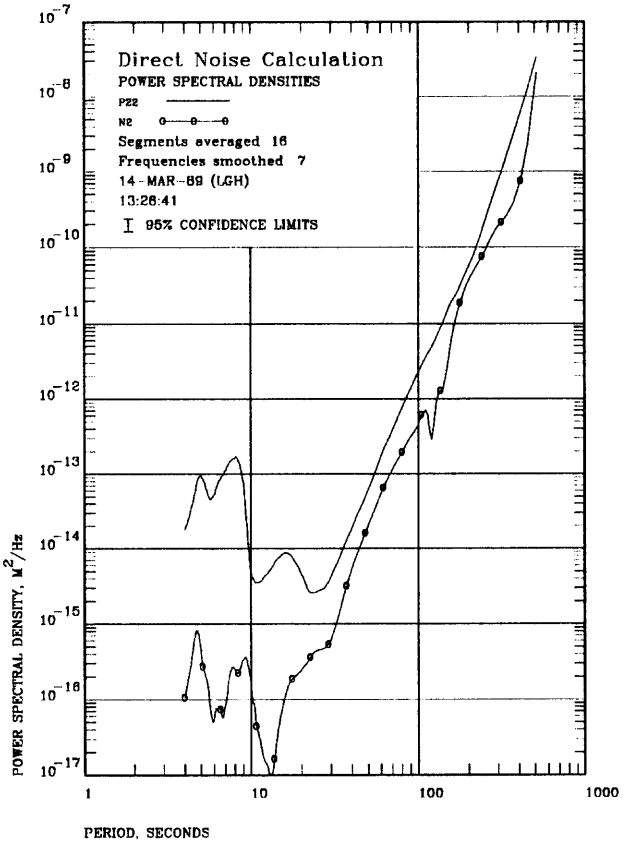

Figure 6.9 N2 PSD estimates with equalization and with supersmoothing.

During the course of this investigation one additional empirical smoothing operation was deemed necessary to make the results palatable. If the sensor being evaluated is a very high quality quiet sensor, the coherent power term in Equations 3.5 and 3.6 approaches the total power term. Due to the impossibility of estimating the PSD's to an infinite precision, the estimate for the coherent power sometimes exceeds the estimate for the total power. The rather disconcerting result is a negative estimate for the noise power under these conditions. For this reason, the noise PSD's presented herein have been calculated by taking the absolute value of Equations 3.5 and 3.6.

The sequence of events in processing data with supersmoothing is as follows. First the channel self PSD's (P_{11} and P_{22}), the real, and the imaginary parts of the cross spectral power are supersmoothed using the process described above. Then the two channel noise spectra (N_1 and N_2) and the coherent power (X) are calculated using Equations 3.3, 3.4, and 3.5 respectively. Finally, N_1, N_2 and X are supersmoothed.

Figures 6.8 and 6.9 contain the results of applying supersmoothing to the test results of Figures 6.5 and 6.6. The overall improvement in the appearance of the spectra is dramatic and the SNR's are nearly what should be expected based on the coherence function analysis of Section 4. In the figures, the visually estimated SNR's range from about 130 to nearly 2000. This is approximately the range predicted by the coherence function which ranges from 0.9832 to 0.9998 thereby indicating that the SNR's must be at least as large as from 49 to over 998.9 (see Table 4.1).

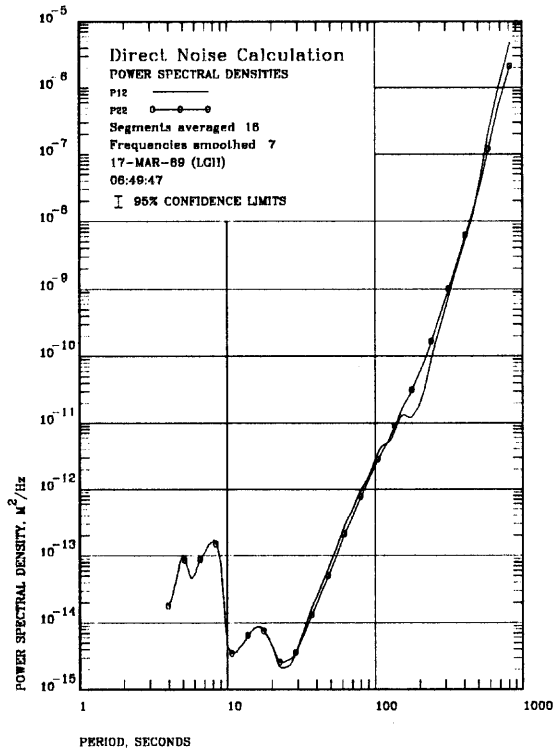

Figure 6.10 Coherent PSD estimate between V349 and V350.

A comparison between the total estimated power output of V350 and the coherent power estimate between the two sensor outputs is shown in Figure 6.10. Careful study of the two PSD estimates reveals that the estimate for the coherent power lies above the estimate for the total power at some points lying above 20 seconds. This is a bit disconcerting but not too worrisome when one superimposes the 95% probable error limits on the PSD estimates. The overlap is well within the possible errors arising from the analysis process. The important observation to make from this data is that most of the power output from sensor V350 is coherent power. Since the PSD estimate above 20 seconds is higher than one should expect for a quiet site, the indication is that there is a source of coherent power within the system over and above the coherent ground motion input to the system. A common source of this type of noise is noise on the common power supply bus which is not properly filtered and isolated at long periods. Therefore, the analysis provides a clue of an area within the CMG-3 system which may be generating excessive noise.

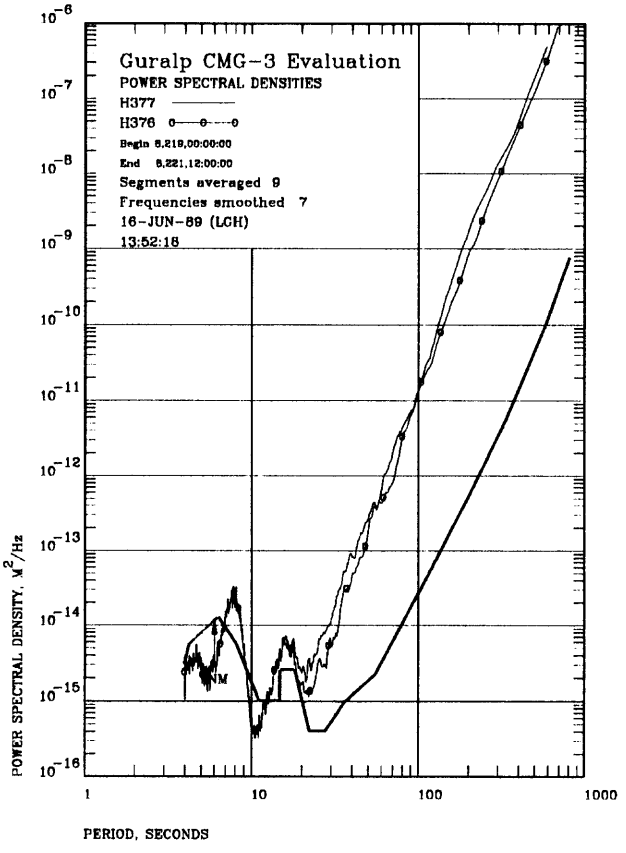

Figure 6.11 PSD estimates (P11 and P22) for Guralp H376 and H377 horizontal sensors.

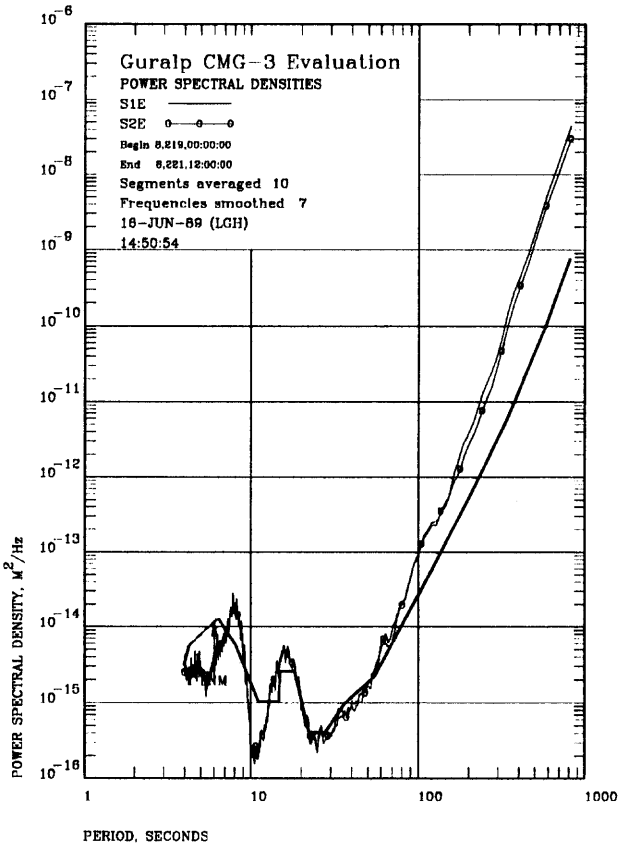

Figure 6.12 PSD estimates (P11 and P22) for Streckeisen SH1 and SH2 horizontal sensors.

Finally the direct model analysis process will be applied to data obtained in side-by-side comparative evaluations of a set of Guralp CMG-3 horizontals and a set of Streckeisen horizontals all four oriented east-west. Figures 6.11 and 6.12 contain PSD estimates for Guralps and Streckeisens respectively. Notice that the CMG-3 sensors are considerably noisier than the Streckeisens at periods above about 15 seconds. Figures 6.13 and 6.14 are the coherence functions for both sets of sensors; the Streckeisens demonstrate considerable coherence even out to 1000 seconds.

Figures 6.15 and 6.16 contain PSD estimates of the total system power as compared to estimates of the noise power in the CMG-3 sensors calculated by the direct method. Notice that the total system power above about 20-25 seconds is almost completely composed of noise because the estimated noise level almost overlays the estimates of the total system power in both sensors.

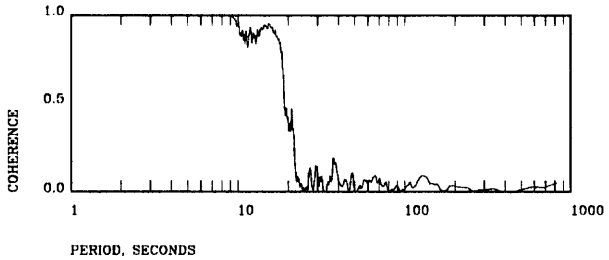

Figure 6.13 Coherence between Guralp H376 and H377 sensors.

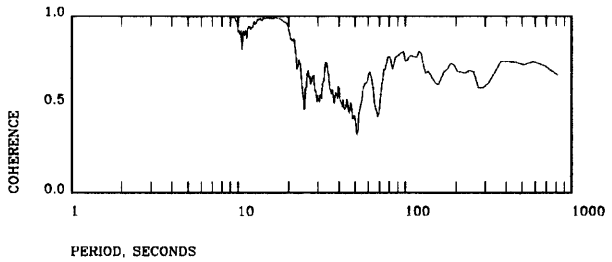

Figure 6.14 Coherence between Streckeisen horizontal sensors.

In contrast, the estimated system noise levels as calculated by the direct method for the Streckeisen sensors shown in Figures 6.17 and 6.18 lies considerably below the total system power estimates for both sensors. Sensor S2E is somewhat quieter at periods beyond 70 seconds but slightly noisier below 30 seconds. This data illustrates a significant asset of the direct method for evaluating relative system performance levels; the noise levels in the sensors can be evaluated independently and realistic estimates for both systems can be made even though they are different.

Finally, Figures 6.19 and 6.20 contain the coherent power estimates as calculated by the direct method between the CMG-3 sensors and between the Streckeisen sensors respectively. The coherent power estimate for the CMG-3's lies far below the total power estimate at periods above 10 seconds indicating that the CMG-3's are failing to resolve true ground motion above 10 seconds. On the other hand, the Streckeisen coherent power estimate lies close to the total system power over the entire range of period, indicating that the Streckeisen systems are sensing true ground motion over the entire range of the spectrum.

The last figure contains an estimate of the probable dynamic range of the direct model when applied to real data. The data in Figure 6.21 was obtained by passing the same digitized signal to both of the inputs of the analysis process; this is equivalent to making $N_1 = N_2 = 0$, or to making N_1 coherent with N_2 in the direct model. Theoretically, the calculated SNR's in both channels should then be infinite. However, visual scaling of the data in Figure 6.21 yields an SNR of only approximately 10^7. The departure from theory is probably due to numerical precision problems such as round off error within the computing process. Regardless of the source of the inaccuracies, the data in Figure 6.21 establishes that the direct model is capable of resolving SNR's which far exceed those likely to be found in real world side-by-side seismometer evaluation data processing.

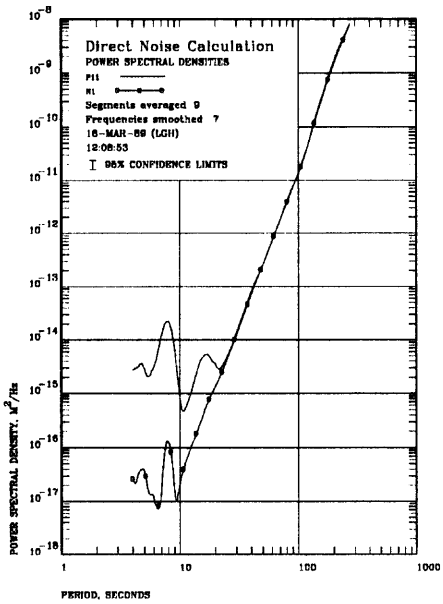

Figure 6.15 Total system power (P11) and noise estimates (N1) for H377.

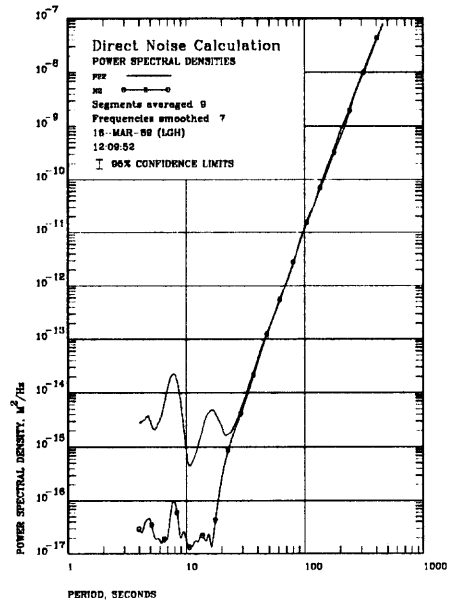

Figure 6.16 Total system power (P22) and noise estimates (N2) for H376.

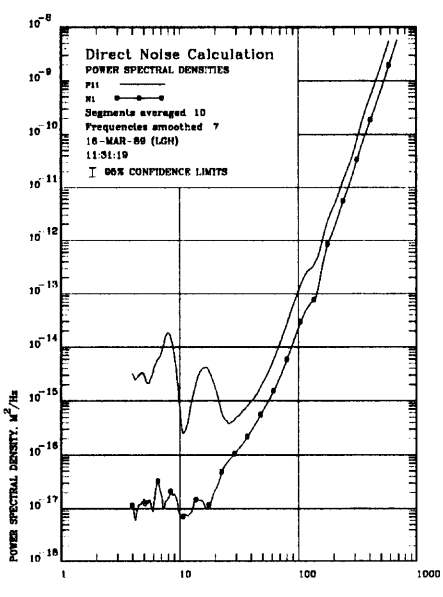

Figure 6.17 Total system power (P11) and noise estimates (N1) for S1E.

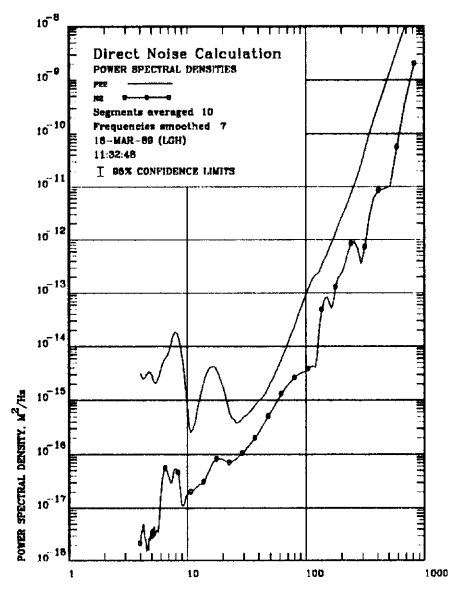

Figure 6.18 Total system power (P11) and noise estimates (N1) for S2E.

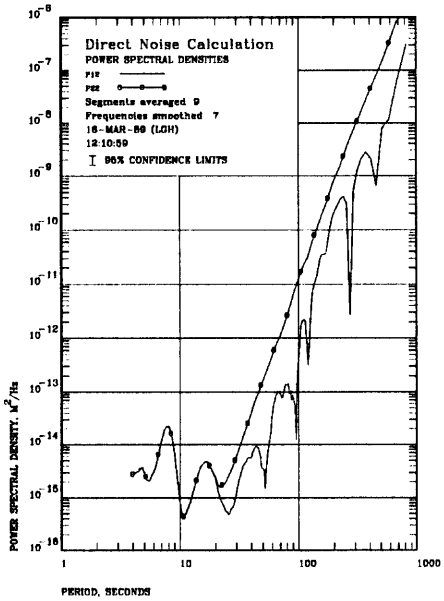

Figure 6.19 Coherent power estimate between H377 and H376.

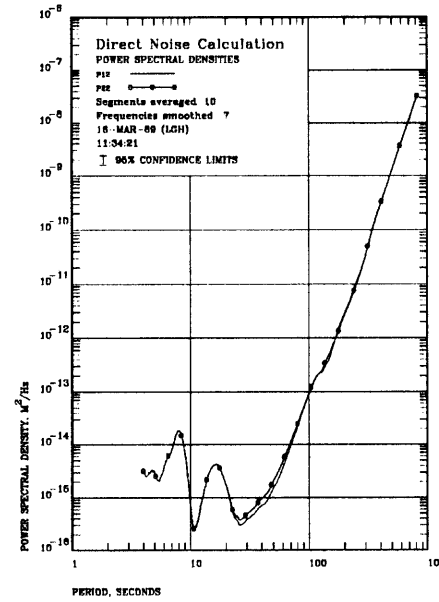

Figure 6.20 Coherent power estimate between S1E and S2E.

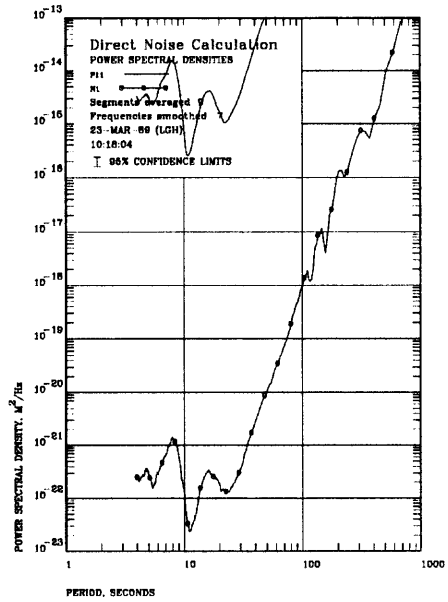

Figure 6.21 Estimate of the probable dynamic range of the direct model analysis process.

7 CONCLUSIONS AND RECOMMENDATIONS

A method for calculating system noise levels directly from the measured PSD outputs of a side-by-side seismometer evaluation has been derived and demonstrated on dummy and real world data. The technique is general in that it requires no special assumptions about the transfer functions other than they be accurately known, and no assumptions are made about the relative noise levels of the two sensors involved. The true meaning of the coherence function in terms of system SNR's and the model parameters of Figure 3.1 has been demonstrated and used as a tool to assist in the noise analysis.

Significant improvements in this analysis process may be possible. In particular, the smoothing operation might be improved by a more exotic model such as a higher order fit to the smoothed data points. The details of the effect of numerical round off have not been investigated and may be important at high SNR's where small differences between large numbers come into play.

8 REFERENCES

Bendat, Julius S., Piersol, Allan G., (1971), "Random Data: Analysis and Measurement Procedures" *John Wiley & Sons, Inc.*

Munk, W. H., Snodgrass, F. E., Tucker, M. J., (1959). "Spectra of low-frequency ocean waves" *Bull. Scripps Inst. Oceonogr., Univ. Calif., 7: 286-362*

Peterson, J., Hutt, Charles R., Holcomb, L. Gary, (1980). "Test and Calibration of the Seismic Research Observatory" *U.S. Geological Survey Open-File Report 80-187, 86 p.*

Press, William H., Flannery, Brian P., Teukolsky, Saul A., Vetterling, William T., (1986). "Numerical Recipes - The Art of Scientific Computing" *Cambridge University Press*

Stearns, Samuel D., David, Ruth A. (1988). "Signal Processing Algorithms" *Prentice-Hall, Inc., Englewood Cliffs, New Jersey*

A APPENDIX

The analysis of Section 3 ignores noise sources which may occur after the band shaping response of the two sensors (H_1 and H_2). Possible sources of post response noise include flat band gain, and noise generated in the instrumentation system used to monitor the sensor performance. Fred Followill of Lawrence Livermore National Laboratories suggested that it would be more realistic to include this noise in the analysis. Figure A.1 contains a linear system model which includes these noise sources.

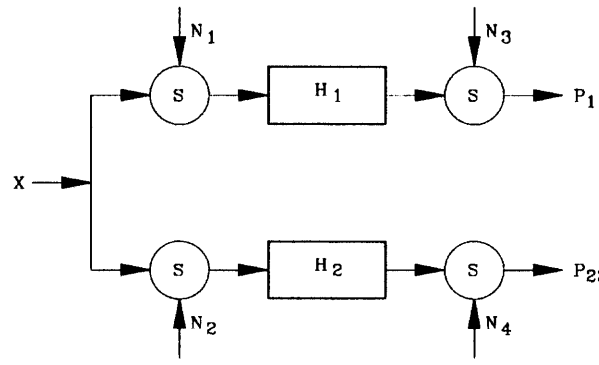

Figure A.1 Linear system model of side-by-side evaluation of two seismometer systems including noise sources introduced by instrumentation after the band shaping response.

In the figure, N_3 and N_4 are the new noise PSD's associated with post response noise sources.

From the model, the power spectral density of the output of system 1 is given by

$$P_{11} = |H_1|^2 [X + N_1] + N_3 \qquad \textit{Equation} \quad A.1$$

and the same quantity for system 2 is

$$P_{22} = |H_2|^2 [X + N_2] + N_4 \qquad \textit{Equation} \quad A.2$$

The cross spectral density between the outputs of the two systems remains unchanged from the previous analysis.

$$P_{12} = H_1 H_2^* X \qquad \textit{Equation} \quad A.3$$

The solution of these equations follows the previous solution. Solve Equation 3.1 for N_1 to yield

$$N_1 = \frac{P_{11} - N_3}{|H_1|^2} - X \qquad \textit{Equation} \quad A.4$$

Substituting for X from Equation A.3 yields

$$N_1 = \frac{P_{11} - N_3}{|H_1|^2} - \frac{P_{12}}{H_1 H_2^*} \qquad \textit{Equation} \quad A.5$$

Similarly, solving Equation A.2 for N_2 and substituting for X from Equation A.3 yields

$$N_2 = \frac{P_{22} - N_4}{|H_2|^2} - \frac{P_{12}}{H_1 H_2^*} \qquad \textit{Equation} \quad A.6$$

In Equations A.5 and A.6 it is evident that, if the levels of instrumentation noise are known, the effects of this noise on the estimates for the sensor self noise can be eliminated by merely subtracting the instrumentation noise levels (N_3 or N_4) from the total output power estimates (P_{11} or P_{22}). Estimates for the instrumentation noise can be obtained by performing appropriate measurements with the inputs to the instrumentation system terminated with proper impedances.

At first examination, the expression for the coherence function appears to be considerably more complicated but it readily simplifies as follows. Start with the definition for the coherence function

$$\gamma^2 = \frac{|P_{12}|^2}{P_{11} P_{22}} \qquad \textit{Equation} \quad A.7$$

Substituting for P_{11}, P_{22}, and P_{12} from equations A.1, A.2, and A.3 respectively yields

$$\gamma^2 = \frac{|H_2 H_2^*|^2}{\{\,|H_1|^2\,[X + N_1] + N_3\}\{\,|H_2|^2\,[X + N_2] + N_4\}} \qquad \textit{Equation} \quad A.8$$

Dividing the numerator and denominator of right side by $|H_1 H_2^*|$ and multiplying out the denominator gives

$$\gamma^2 = \frac{X^2}{X^2 + X[N_1 + N_2] + N_1 N_2 + \frac{N_3[X + N_2]}{|H_1|^2} + \frac{N_4[X + N_1]}{|H_2|^2} + \frac{N_3 N_4}{|H_1|^2 |H_2|^2}} \qquad \textit{Equation} \quad A.9$$

Refactoring the denominator yields

$$\gamma^2 = \frac{X^2}{X^2 + X\left[N_1 + N_2 + \frac{N_3}{|H_1|^2} + \frac{N_4}{|H_2|^2}\right] + \left[N_1 N_2 + \frac{N_2 N_3}{|H_1|^2} + \frac{N_1 N_4}{|H_2|^2} + \frac{N_3 N_4}{|H_1|^2 |H_2|^2}\right]} \qquad \textit{Equation} \quad A.10$$

Regrouping the linear coefficient of X and factoring the constant term in the denominator we have

$$\gamma^2 = \frac{X^2}{X^2 + X\left\{\left[N_1 + \frac{N_3}{|H_1|^2}\right] + \left[N_2 + \frac{N_4}{|H_2|^2}\right]\right\} + \left[N_1 + \frac{N_3}{|H_1|^2}\right]\left[N_2 + \frac{N_4}{|H_2|^2}\right]} \qquad \textit{Equation} \quad A.11$$

If we let

$$N_1' = N_1 + \frac{N_3}{|H_1|^2} \qquad \textit{Equation} \quad A.12$$

and

$$N_2' = N_2 + \frac{N_4}{|H_2|^2} \qquad \textit{Equation} \quad A.13$$

Equation A.11 becomes

$$\gamma^2 = \frac{X^2}{X^2 + X[N_1' + N_2'] + N_1' N_2'} \qquad \textit{Equation} \quad A.14$$

This equation has the same form as Equation 4.3 in the original derivation of the model expression for the coherence function contained in Section 4 above. The similarity in the two models is obvious if the post response instrumentation noise shown in Figure A.1 is referred to the input of the sensor system as shown in Figure A.2 below.

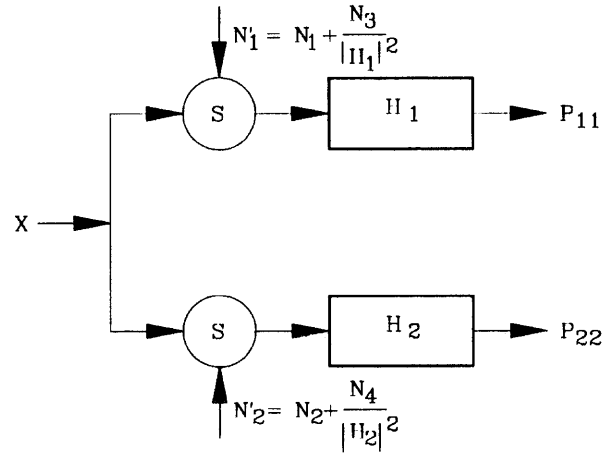

Figure A.2 Linear system model of side-by side evaluation of two seismometer systems including noise sources introduced by instrumentation after the band shaping response with the instrumentation noise referred to the sensor input.

Therefore, the portion of the derivation in Section 4 following Equation 4.3 leading to the hyperbolic relationship between the signal-to-noise ratio and the coherence function can be applied to the more general model being analyzed in this appendix merely by substituting

$$N_1 = N_1' - \frac{N_3}{|H_1|^2} \qquad \textit{Equation} \quad A.15$$

and

$$N_2 = N_2' - \frac{N_4}{|H_2|^2} \qquad \textit{Equation} \quad A.16$$

in Equations 4.4 through 4.7.

The hyperbolic curves of Figures 4.1 and 4.2 remain applicable to the general case as long as the SNR's read from the curve for a given coherence are interpreted as being composed of incoherent noise from two sources. The minimum sensor SNR is probably greater than indicated by the curves in the two figures because post response noise degrades the measured coherence.

In summary, if instrumentation noise levels are significantly high, their effects should be considered in analyzing the data via the direct method presented in this report. It is relatively easy to correct the calculated sensor noise levels for the effects of instrumentation noise using Equations A.5 and A.6.